Supporting information

NIR-activated dual-mode oxygen-generating and -delivering nanoplatform for enhanced photodynamic therapy of cervical cancer†

Jiaxing Li ‡[a], Chenyang Chu [b], Lijun Zhu [c], Zhong Du [c], Yaqi Cui [a,d], Jiabao Xiong [c], Chi Zhang [c], Yuxiang Gao [c], Biao Dong *[a,d], Nuernisha Alifu *[a,c,e]

[a]Department of Medical Engineering and Technology, Xinjiang Medical University, Urumqi 830011, China.

[b]Department of Gynecology, The First Affiliated Hospital of Xinjiang Medical University, State Key Laboratory of Pathogenesis, Prevention and Treatment of High Incidence Diseases in Central Asia, Urumqi 830054, China.

[c]The Second Affiliated Hospital of Xinjiang Medical University, The Second School of Clinical Medicine, Xinjiang Medical University, Urumqi 830054, China

[d]State Key Laboratory on Integrated Optoelectronics, College of Electronic Science and Engineering, Jilin University, Changchun 130012, China

[e]Scientific Research and Innovation Center, Xinjiang Medical University, Urumqi 830054, China.

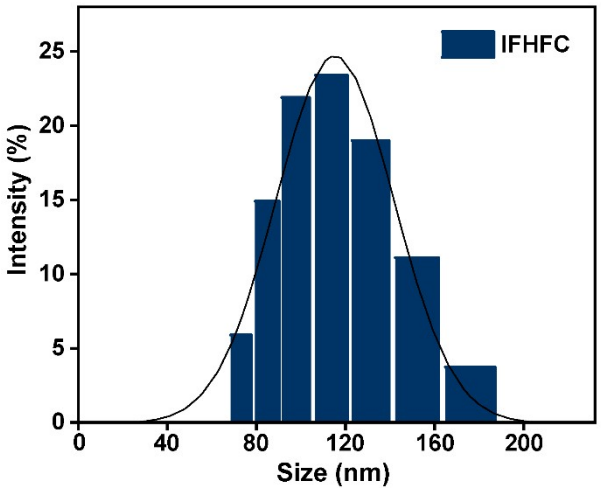

Fig. S1 Hydrodynamic size distribution of IFHFC NPs.

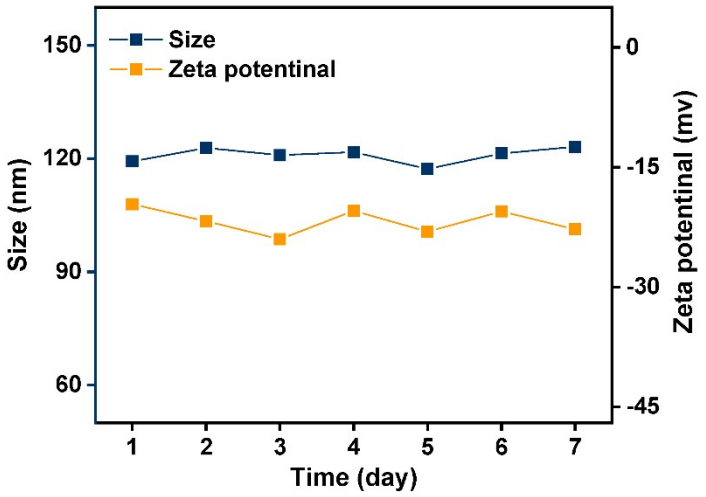

Fig. S2 Stability of zeta potential and hydrodynamic diameter of IFHFC NPs in aqueous solution over 1–7 days.

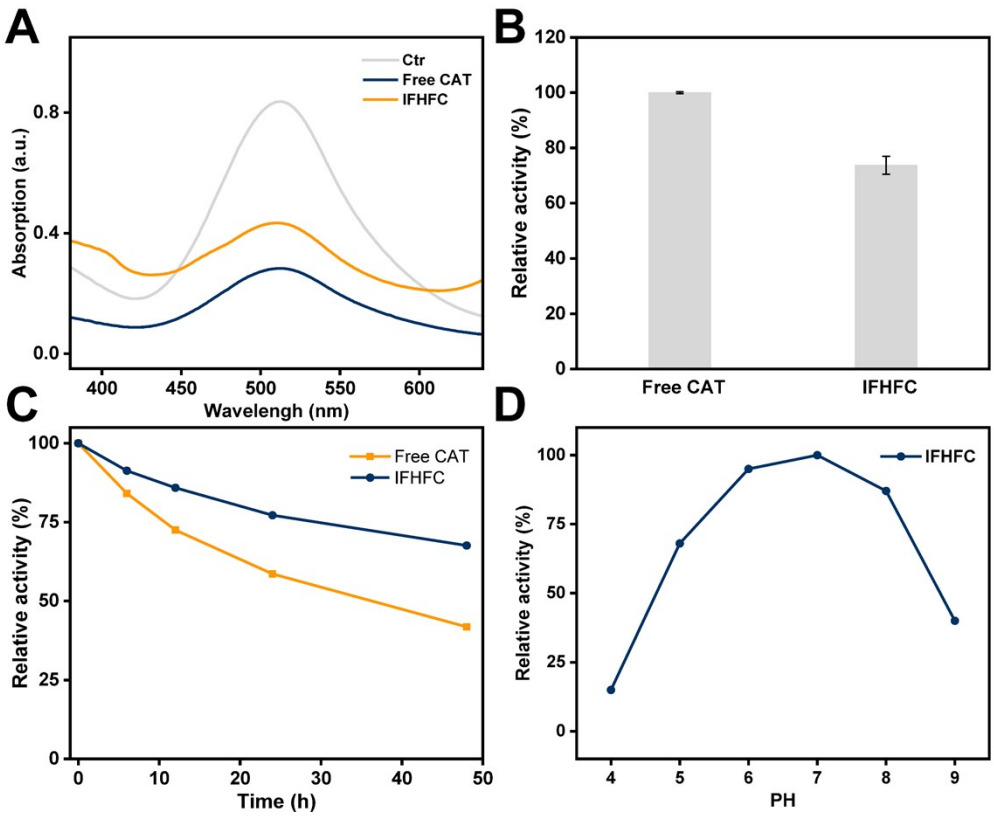

Fig. S3 (A) UV–vis absorbance changes used to evaluate the catalytic activity of free CAT and CAT in IFHFC. (B) Quantitative analysis of CAT activity based on the UV–vis assay in panel A, showing the relative activity of free CAT and IFHFC (free CAT set as 100%). (C) Long-term stability of CAT activity over 0–48 h. (D) Relative CAT activity of IFHFC at different pH values.

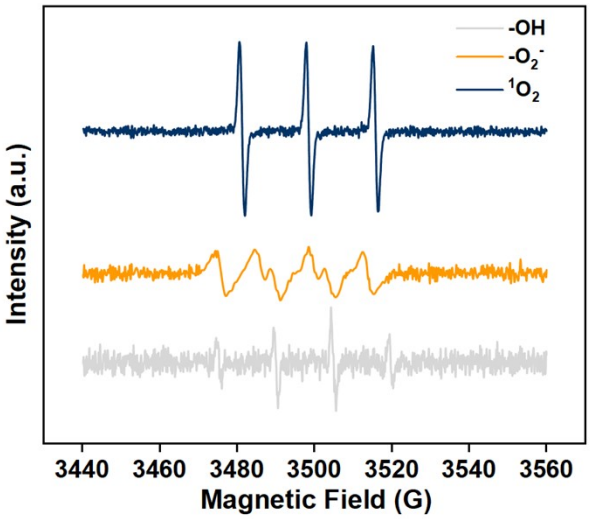

Fig. S4 Electron spin resonance (ESR) spectra of different reactive oxygen species (ROS)

generated by IFHFC under laser irradiation ($^1O_2$, $\cdot O_2^-$, and ·OH).

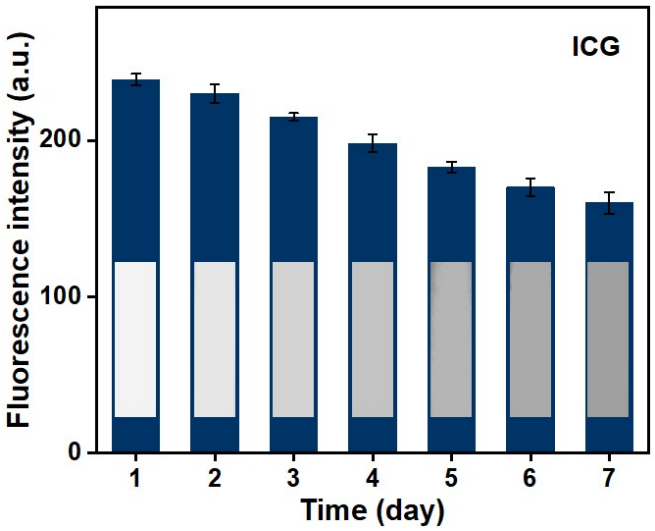

Fig. S5 Fluorescence intensity stability of free ICG aqueous solution under 808 nm irradiation (power density 1 W cm^{-2}).

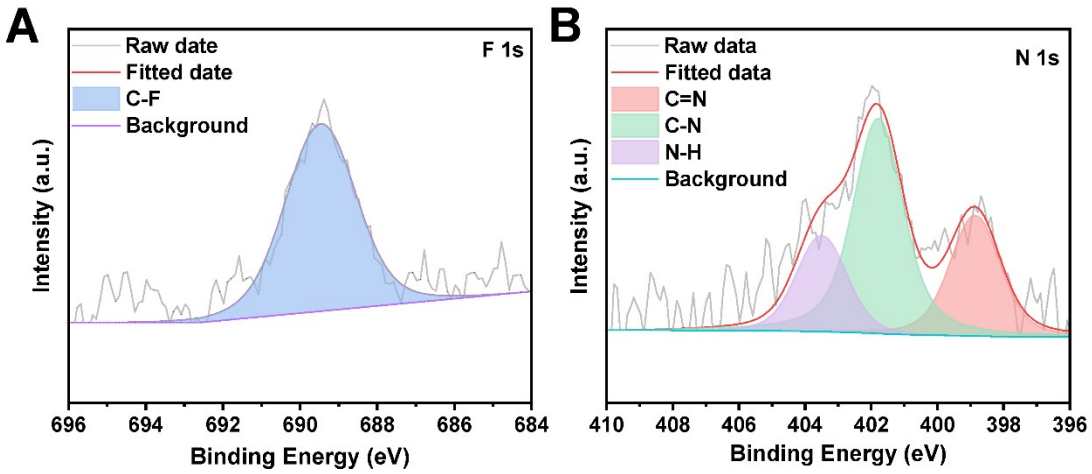

Fig. S6 XPS analysis of F and N in IFHFC NPs

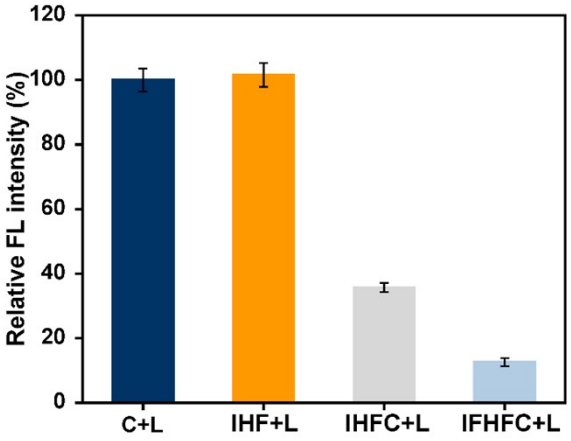

Fig. S7 Quantitative analysis of intracellular fluorescence intensity of the hypoxia probe $[Ru(dpp)_3]Cl_2$ in HeLa cells under different treatments.

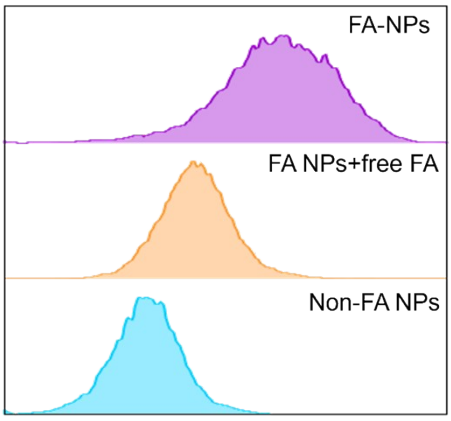

Fig. S8 Flow cytometry histograms of cellular uptake for FA-NPs, FA-NPs with free FA blocking, and non-FA NPs.

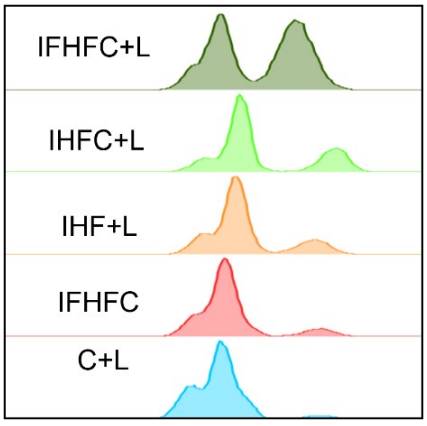

Fig. S9 Flow cytometric analysis of intracellular ROS levels in different treatment groups.

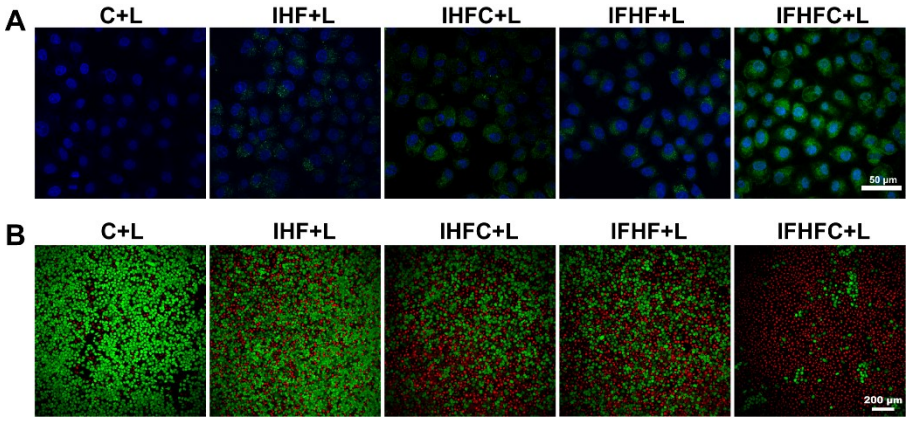

Fig. S10 (A) Confocal fluorescence microscopic images of HeLa cells stained with DCFH-DA under different treatment conditions (808 nm, 1.0 W cm^{-2}, 5 min). Scale bar : 50 μm. (B) Confocal fluorescence microscopic images of HeLa cells stained with Calcein-AM/PI to evaluate phototherapeutic efficacy (808 nm laser, 1.0 W cm^{-2}, 5 min). Scale bar : 200 μm.

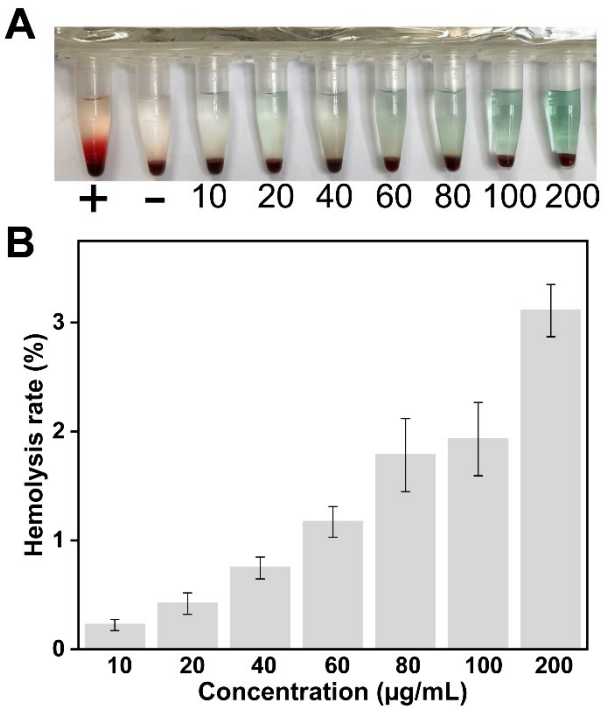

Fig. S11 (A) Photographs and (B) quantitative hemolysis ratios of red blood cells after exposure to IFHFC NPs at increasing concentrations (10–200 μg/mL). Physiological saline and deionized water (DIW) served as the negative and positive controls, respectively.

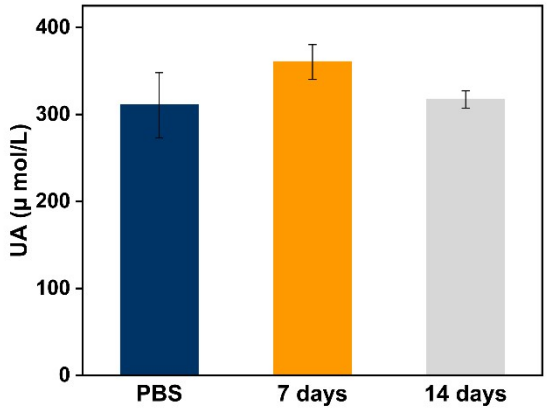

Fig. S12 *In vivo* toxicity evaluation of IFHFC NPs based on changes in hematological parameters and serum biochemistry (UA) on days 7 and 14 post-administration.

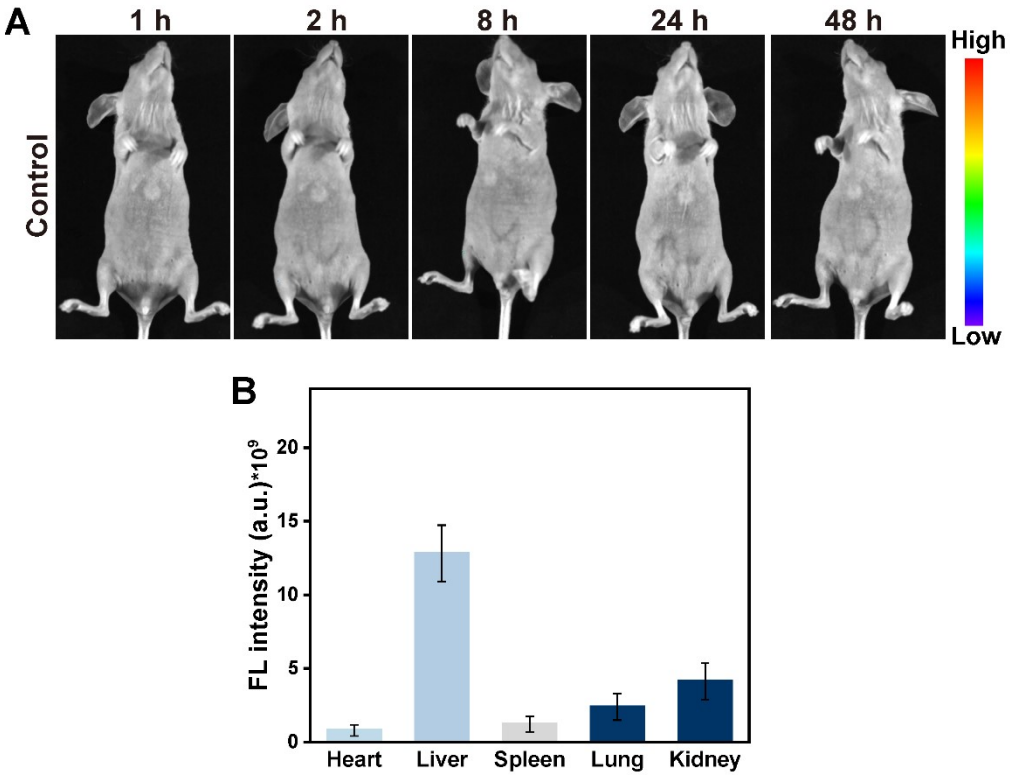

Fig. S13 (A) PBS control group in the in vivo biodistribution study, imaged at the indicated time points. (B) Quantitative fluorescence analysis of major organs from mice treated with IHFFC NPs.

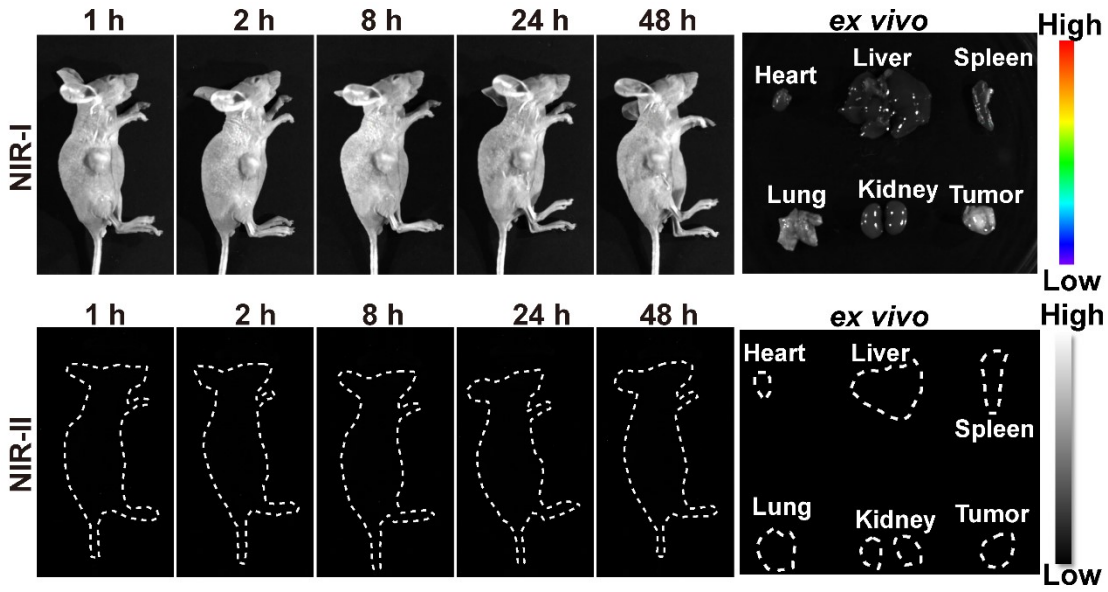

Fig. S14 NIR-I and NIR-II fluorescence imaging of tumors at indicated time points after tail-vein injection of 1× PBS (control), and *ex vivo* fluorescence images of major organs and tumors at 72 h.

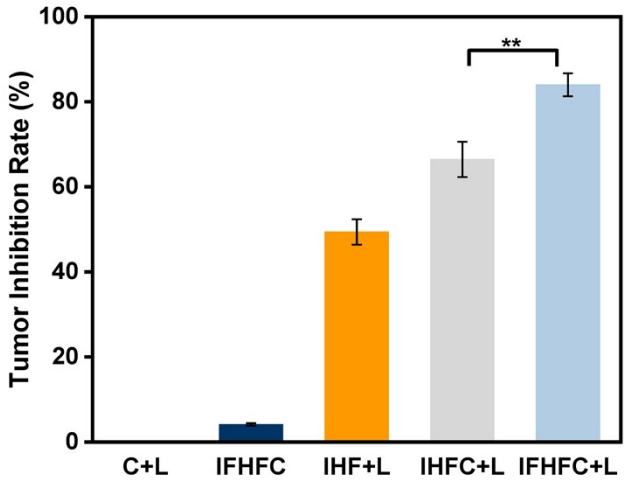

Fig. S15 Tumor inhibition rate of each treatment group. Data are presented as mean ± standard deviation. **p < 0.01.

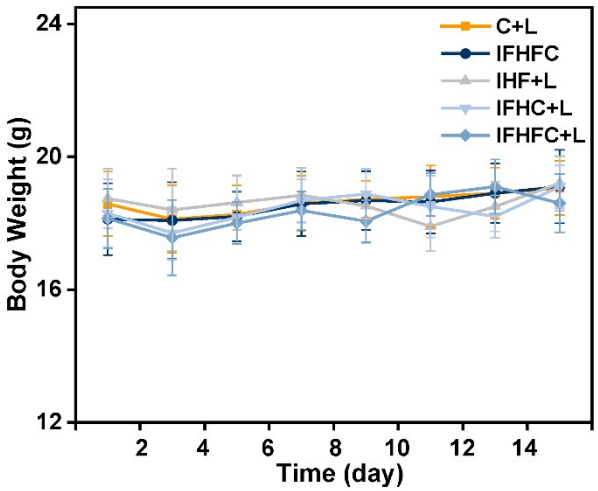

Fig. S16 Average body weight of mice in each group during the treatment period.

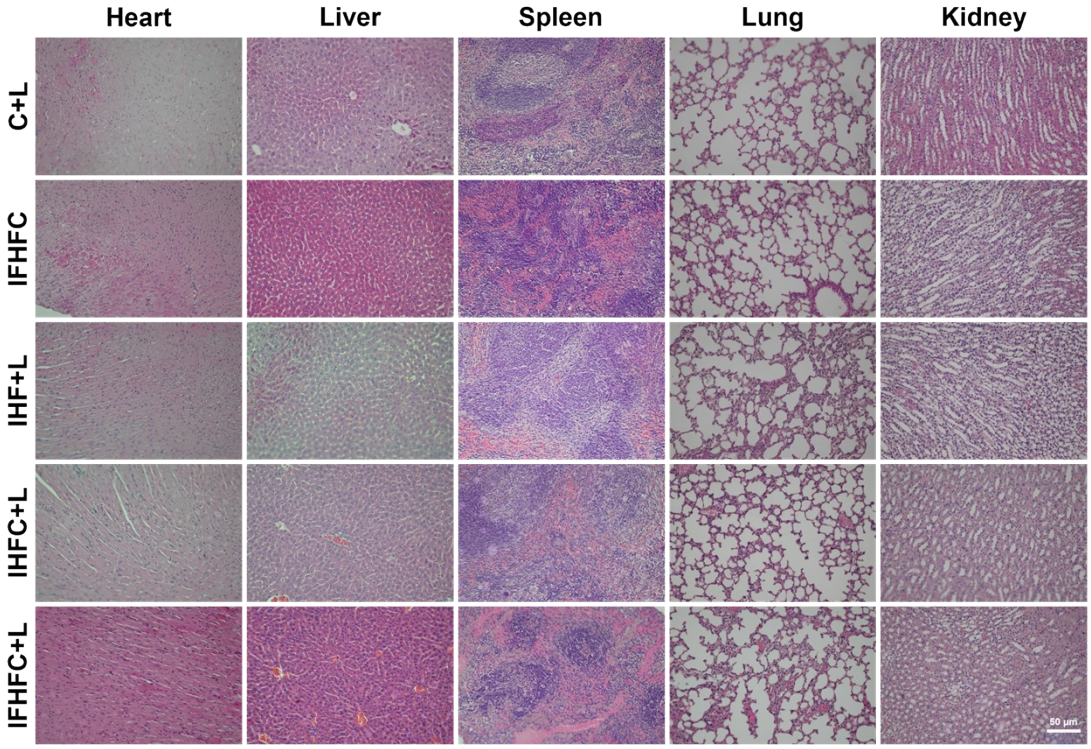

Fig. S17 H&E staining images of the main organs (heart, liver, spleen, lung, kidney) of mice after different intervention treatments (scale bar: 50 μm).

Component	Drug Loading Content (DLC, %)	Encapsulation Efficiency (EE, %)
PFH	24.3%	83.2%
ICG	3.88%	96.3%

Table S1 Drug loading capacity and efficiency of the IFHFC NPs.